Supporting Information

Effects of Bubbles on the Electrochemical Behavior of Hydrogen-Evolving Si Microwire Arrays Oriented Against Gravity

Paul A. Kempler[1], Robert H. Coridan[2], Nathan S. Lewis[1,3*]

[1]Division of Chemistry and Chemical Engineering, 127-72, 210 Noyes Laboratory, California Institute of Technology, Pasadena, CA 91125

[2]Department of Chemistry and Biochemistry, University of Arkansas, Fayetteville, Arkansas 72701

[3]Beckman Institute, California Institute of Technology, Pasadena, CA 91125

*Corresponding Author: nslewis@caltech.edu

Table of Contents

Extended experimental methods

Materials: All chemicals were commercially available and used as received. Fe(II) sulfate heptahydrate (ACS Reagent, >99%), Fe(III) sulfate hydrate (97%) and 1,10-phenanthroline (>99%) were obtained from Sigma-Aldrich, gallium-indium eutectic (GaIn, 99.99%, metals basis) was obtained from Alfa Aesar, and concentrated ammonium hydroxide (NH_4OH, 28%-30%) was obtained from JT Baker. Hydrochloric acid (HCl, ACS grade 36.5-38%), acetone, and isopropyl alcohol were obtained from Millipore. Buffered oxide etchant (6:1 (v/v) 40% NH_4F to 49% HF) was obtained from Transene Inc and hydrogen peroxide (H_2O_2, ACS grade 30%) was obtained from Macron Chemicals. Hydroxylamine sulfate (>98%) was obtained from TCI America. Sulfuric acid (H_2SO_4, TraceMetal grade) was obtained from Fisher Scientific and diluted to 0.50 M with water having a resistivity of 18.2 MΩ·cm, obtained from a Millipore deionized (DI) water system. N-type Si wafers with a resistivity < 0.005 Ω-cm and diameters of 100 mm, thicknesses of 525 μm, and <100> orientation, were obtained from Addison Engineering. Nafion™ 117 was obtained from Fuel Cell Store.

Preparation of μW substrates: Silicon wafers were cleaned with acetone and isopropyl alcohol, exposed to a hexamethyldisilazane primer, and spin-coated with S1813 photoresist (Shipley) at 4000 rpm. The resist layer was photolithographically patterned via UV-exposure through a chrome mask which had a square grid of circular holes 3 or 6 μm in diameter and 11, 14, or 28 μm in spacing. Al_2O_3 etch masks, 125 nm in thickness, were evaporated into the exposed hole array via electron beam evaporation at 1 Å s^{-1}. Substrates were cleaved, mounted onto a 6" diameter Si carrier wafer with thermally conductive oil, and loaded into an Oxford Instruments Dielectric System 100 ICP-RIE. Microwires were formed via deep reactive-ion etching, DRIE, of Si at -120-

130°C in a SF_6/O_2 plasma at a capacitively coupled power of 3-5 W and an inductively coupled power of 900 W. Silicon was cleaned prior to metallization via a modified Radio Corporation of America (RCA) standard clean 1 (5:1:1 (vol) H_2O:NH_4OH:H_2O_2 at 70-75 °C) for at least 10 min followed by an RCA standard clean 2 (6:1:1 (vol) H_2O:HCl:H_2O_2 at 65-70 °C) for at least 10 min. The samples were dipped in HF between the cleaning steps, which also resulted in the removal of the Al_2O_3 etch mask.

Mass transport measurements: The thickness of the diffusion layer was measured via spectrophotometric determination of Fe^{2+} in a Shimadzu Solid Spec 3700 ultraviolet-visible spectrometer, following complexation with 1,10-phenanthroline in 0.50 M H_2SO_4(aq) and mixing the solution with 2.3 mL of 0.2 M sodium acetate (aq) to bring the pH to 4-4.5.[1] The testing cell was set up in a nominally identical manner to the cell used for HER testing, with the addition of 8.80 mL of 0.100 M Fe^{3+}(aq), as Fe(III) sulfate, in 0.50 M H_2SO_4(aq) to the 50 mL electrolyte prior to testing to an initial $C^{*}_{Fe^{3+}}$ = 0.0150 M. The precise concentration of the ferric sulfate stock solution was determined via spectrophotometry, following reduction with hydroxylamine, and assuming a molar extinction for tris(1,10-phenanthroline)iron(II) of 1.10 x 10^4 M^{-1} cm^{-1}.[1,2] A diffusion coefficient of Fe^{3+}(aq) of 5.5 x 10^{-6} cm^2 s^{-1} was assumed in calculating boundary layer thicknesses, assuming planar diffusion (Equation 1). The value of $C^{*}_{Fe^{3+}}$ was adjusted to be the last recorded concentration of Fe^{2+}(aq), with the concentration of Fe^{2+}(aq) not changing by more than 4% during an individual electrolysis.

Impedance spectroscopy: Nyquist plots were prepared by taking an average of 2 consecutive impedance measurements at a given frequency, at a sampling rate of 6 points per decade. Galvanostatic impedance measurements were performed using a sinusoidal current wave of

0.100 μA at a frequency of 50 kHz superimposed over a constant J_{H_2}. At high frequencies, Z(Re) was constant but Z(Im) consistently trended towards positive values. Such an impedance response, which is equivalent to the behavior of a negative capacitance, has previously been reported for silicon-metal contacts under forward bias at the high frequency limit.[3]

Electrochemical Testing with High-Speed Microscopy: Electrodes for microscopy experiments were made by procedures that were mutually consistent with those used to make electrodes for the other experiments. Si microwire samples were mounted to wires by first scribing In-Ga eutectic into the back of the chip, then adhering the samples to a coiled wire with conductive Ag paint (SPI). The wire was secured in a length of flexible PVC shrink tubing, then sealed with epoxy (Loctite Hysol 9460) to leave exposed only the active electrode area. The electrode area was measured with a flatbed scanner in conjunction with the ImageJ software package. High-speed microscopy experiments were performed in 0.50 M H_2SO_4(aq) in an HDPE electrochemical cell with a glass cover. The imaging system consisted of a microscope (Olympus BX-53) with a 5x objective, a LED reflectance illuminator (Prior Scientific), and a high-speed camera (Fastec Imaging). The working electrode was positioned under the objective lens with the microwires oriented vertically. The electrode depth was maintained at 8 mm under the electrolyte level to maintain a consistent hydrostatic pressure between experiments. The counter electrode consisted of a Pt wire in a glass tube separated from the rest of the electrolyte by a Nafion membrane, to prevent O_2 crossover. A Ag/AgCl (sat. KCl) reference electrode was used to monitor the working electrode potential during the chronopotentiometry measurements. Between microscopy experiments, the electrolyte was purged by electrolysis via a Pt wire cathode (and the counter electrode as the anode) performing H_2 evolution at 300 mA.

Calculations of Growth Coefficients: Radius versus time data for individual bubbles measured via high-speed microscopy were fit to a model for diffusive growth of a gas bubble in a supersaturated medium (Equation S1).[4,5]

$$R(t) = \tilde{b}\left(D_{H_2} t\right)^{1/2} \tag{S1}$$

where $D_{H_2} = 4.5 \times 10^{-5}$ cm^{-2} s^{-1} is the diffusivity of H_2 in solution and $\tilde{b}$ is the dimensionless growth coefficient. When the driving force for bubble growth is small, the effects of advection at the growing surface can be ignored, such that analytical expressions can be derived relating b\tilde to $C_{H_2(aq)}$.[4] A self-consistent requirement for neglecting the effects of advection is that the Péclet number, which expresses the ratio of advective and diffusive growth, is < 1. For $\tilde{b} > 1$ this condition does not hold and growth coefficients were thus not directly related to $C_{H_2(aq)}$.[4]

Calculation of Weighted Mean Bubble Diameter: The thickness of the gas bubble layer was variable in time and with position on the electrode surface. The mean bubble diameter, *d*, weighted by the fraction of surface obscured by an individual bubble, was calculated as an approximation of the instantaneous gas bubble layer thickness (Equation S2).

$$\bar{d}_w = \frac{\pi}{A}\sum_i^n d_i \times \frac{d_i^2}{4} \tag{S2}$$

Where *A* is the geometric surface area of the electrode, the surface is assumed to be obscured by the projected area of the bubble, and the contact angle is assumed to be large such that the height of the bubble is approximately equal to the diameter.

Supporting Figures

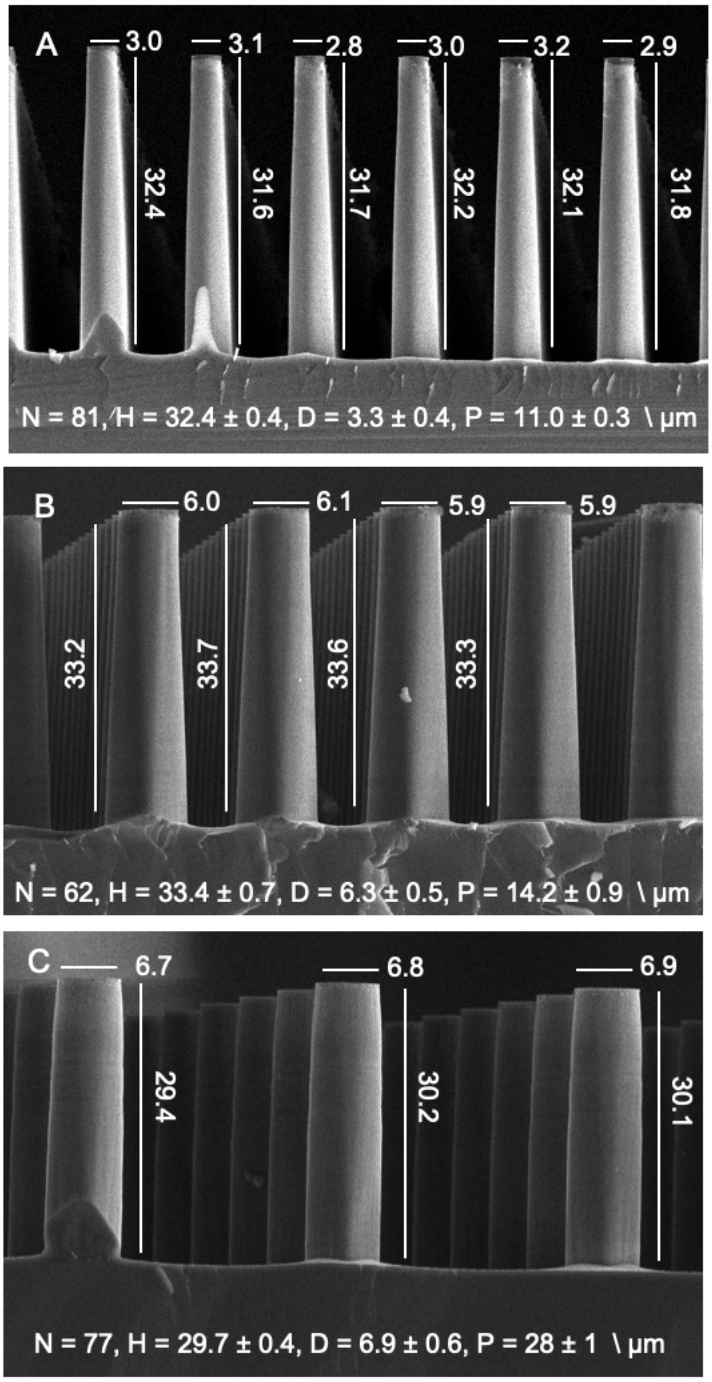

Figure S1: Representative cross section SEM images for µW 3|11 (A), µW 6|14 (B), and µW 6|28 (C) samples. Statistics for wire height, H, and tip diameter, D, and pitch, P, as measured from N wires in multiple SEM images are presented at the bottom of each image along with the standard deviation across the measurements.

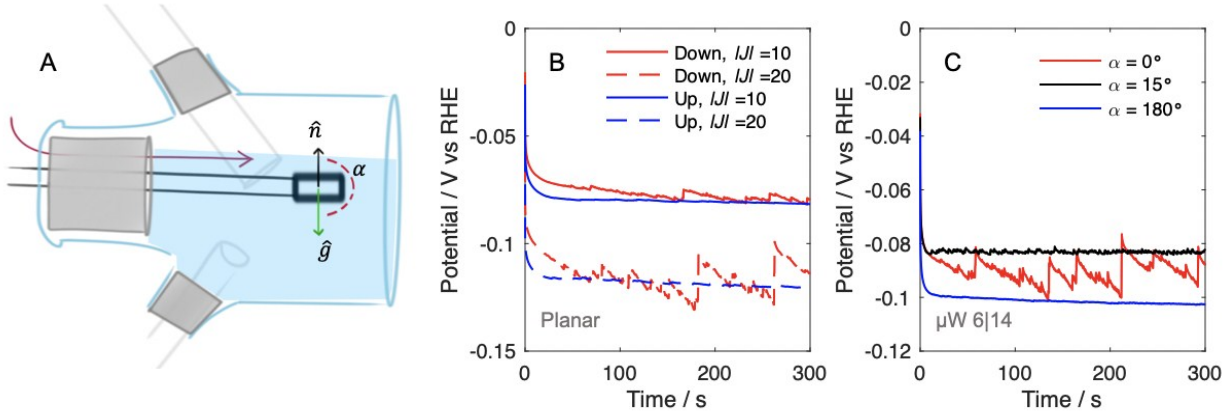

Figure S2: (A) Schematic of cell used to test electrodes as both upward-facing and downward facing cathodes. (B) Potential versus time data for a planar n^+-Si/Ti/Pt electrode as a function of current density and orientation versus the gravitational vector in stagnant, 0.50 M H_2SO_4(aq) under 1-atm H_2 (g) (B) Potential versus time data for a n^+-Si/Ti/Pt μW 6|14 electrode at $|J_{H_2}| = 20$ mA cm^{-2}.

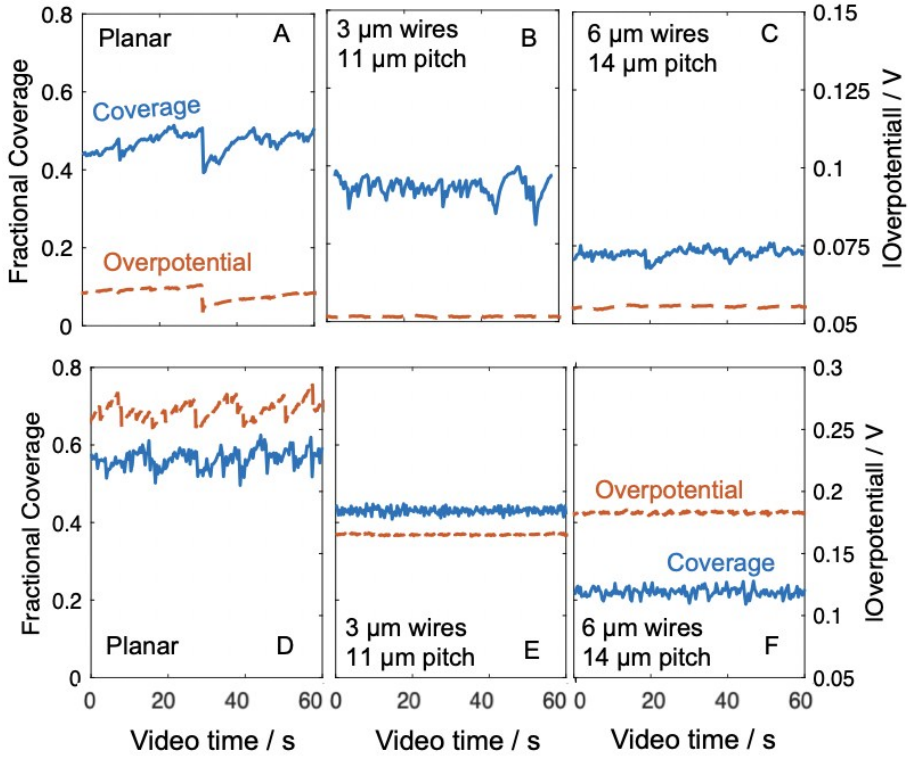

Figure S3: Comparison of fractional gas coverage of downward-facing cathodes, with 15 degrees of tilt, during a representative 60 s of a constant current experiment, operating at (A-C) -10 mA cm^{-2} and (D-F) -70 mA cm^{-2}, relative to the absolute overpotential for the HER in 0.50 M H_2SO_4(aq) as a function of time.

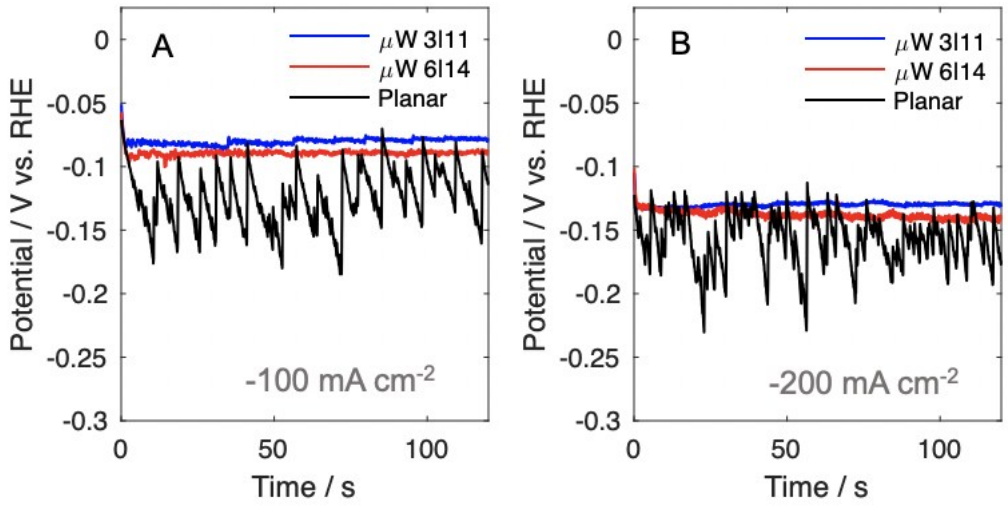

Figure S4: IR-corrected chronopotentiometry data for n^+-Si/Ti/Pt cathodes at α = 15° in 0.50 M H_2SO_4(aq) at -100 mA cm^{-2} (A) and -200 mA cm^{-2} (B).

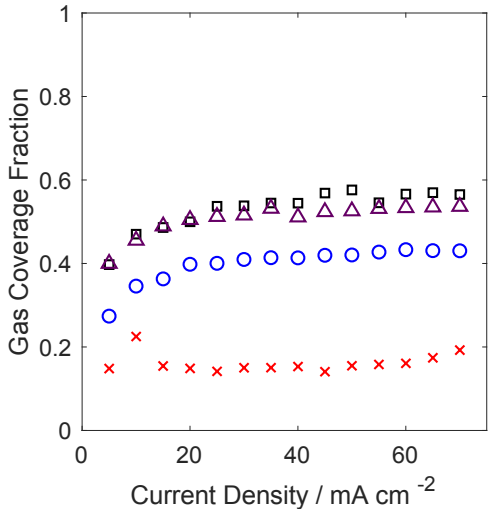

Figure S5: Relationship between the mean gas coverage and current density for various downward-facing hydrogen-evolving cathodes in 0.50 M H_2SO_4(aq). Planar silicon: black squares; μW 3|11: gray diamonds; μW 6|14: red x's; μW 6|28: blue circles.

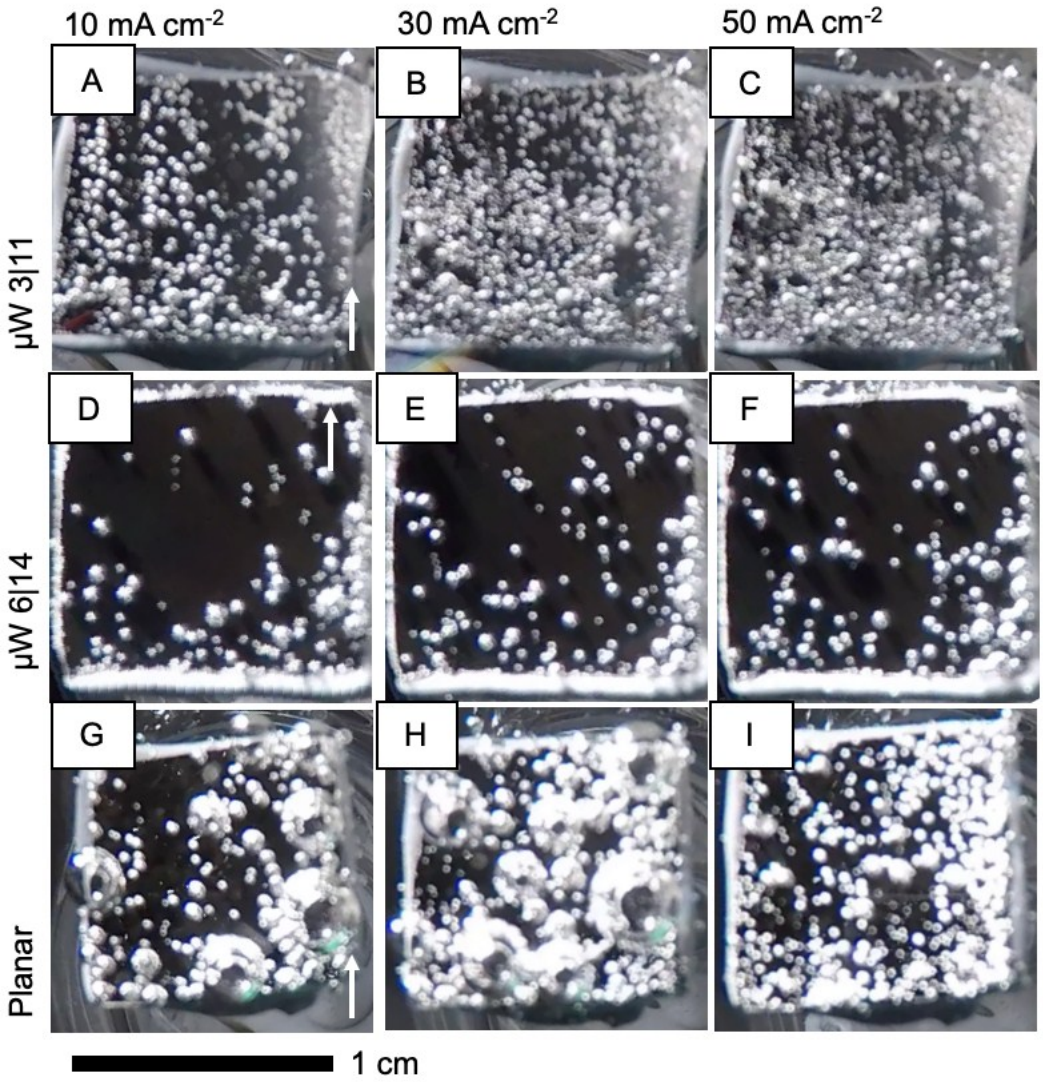

Figure S6: Representative images from Movie S1, recorded at downward facing μW 3|11 (A-C), μW 6|14 (D-F) and planar (G-I) cathodes as a function of $|^{J_{H_2}}|$ at α = 15° in 0.50 M H_2SO_4(aq).

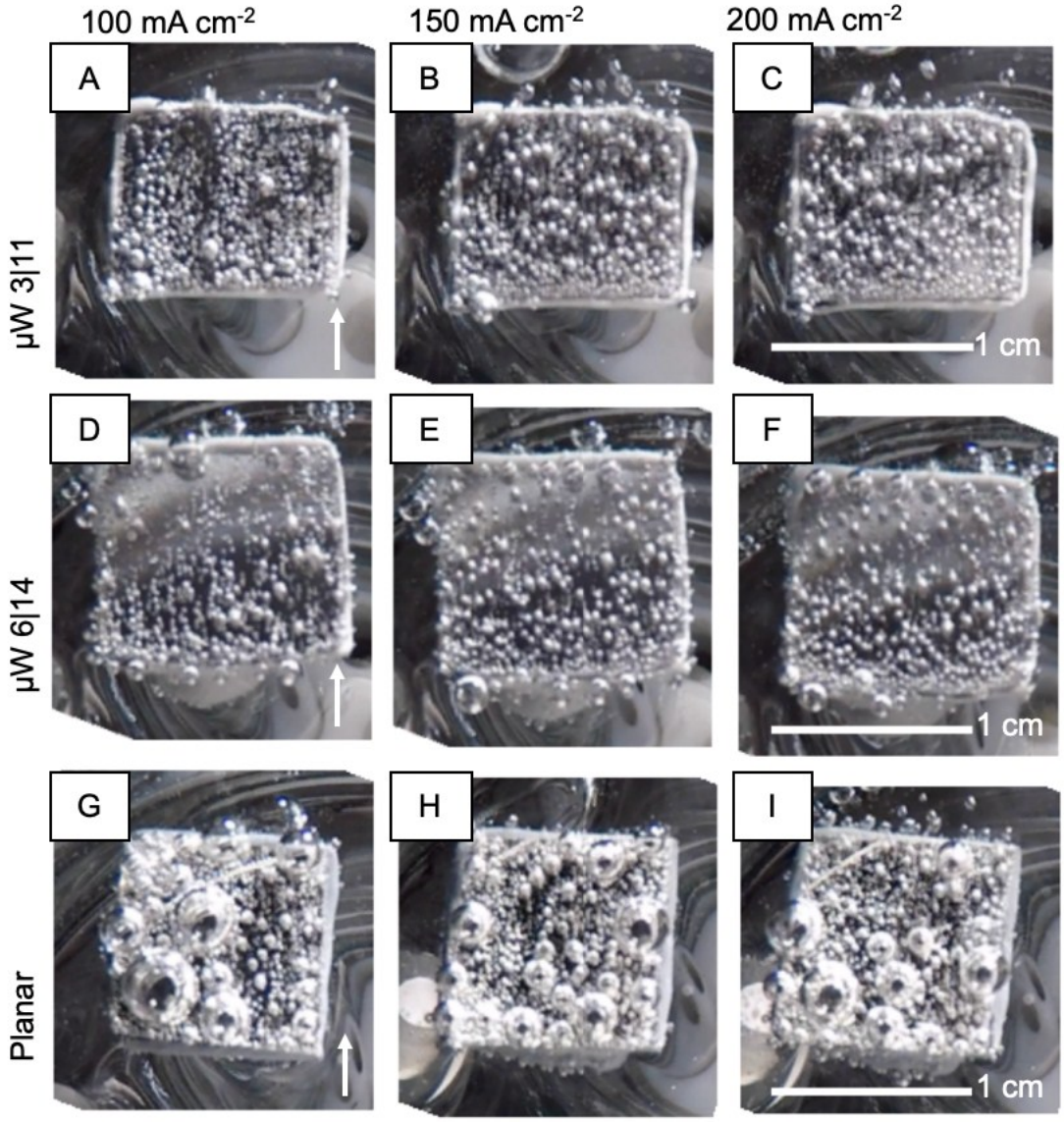

Figure S7: Representative images from Movie S2, recorded at downward facing μW 3|11 (A-C), μW 6|14 (D-F) and planar (G-I) cathodes as a function of $\left|J_{H_2}\right|$ at α = 15° in 0.50 M H_2SO_4(aq).

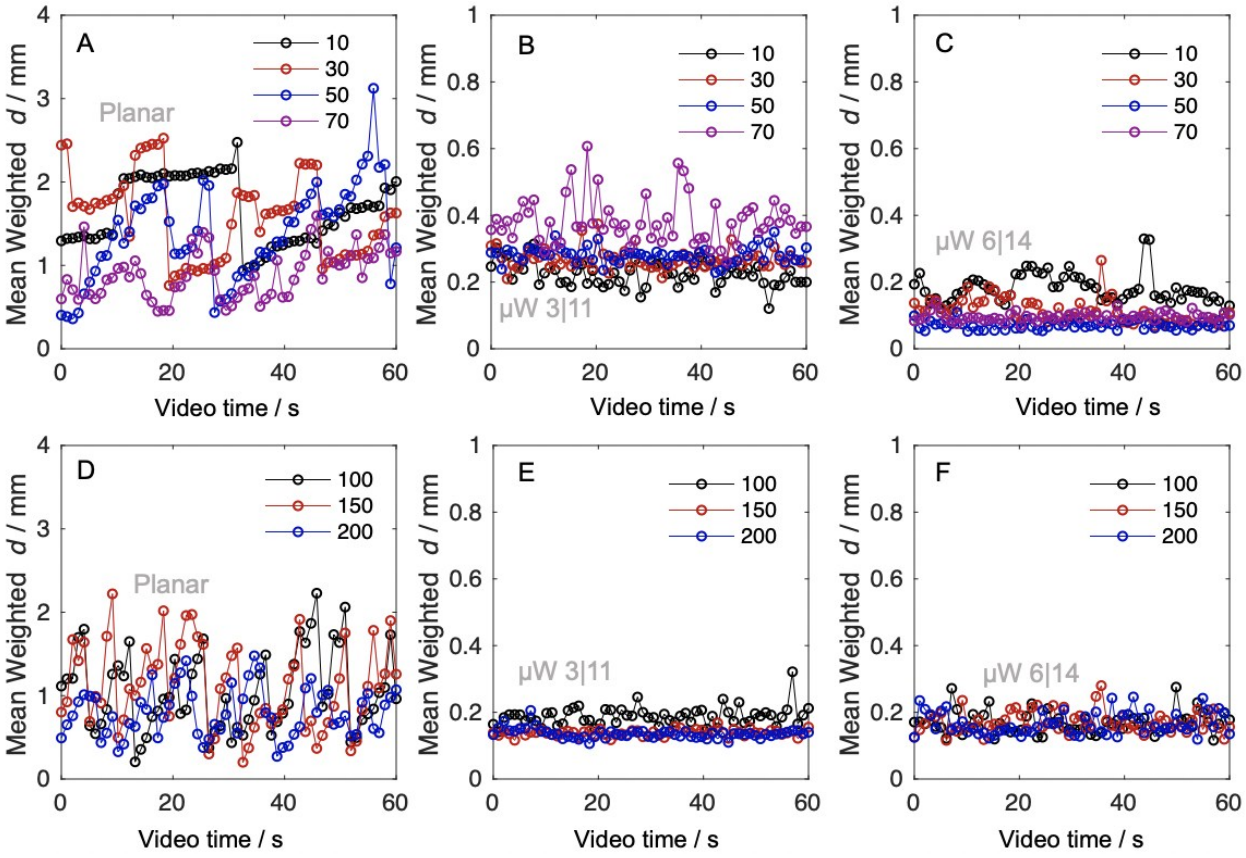

Figure S8: Weighted mean bubble diameters (Equation S2) versus video time at $|J_{H_2}|$ = 10-70 mA cm^{-2} (A-C) and $|J_{H_2}|$ = 100-200 mA cm^{-2} (D-F) as measured at n$^+$-Si/Ti/Pt planar, (B,E) μW 3|11 (A,D), and μW 6|14 electrodes (C,F) in 0.50 M H_2SO_4(aq) at α = 15°.

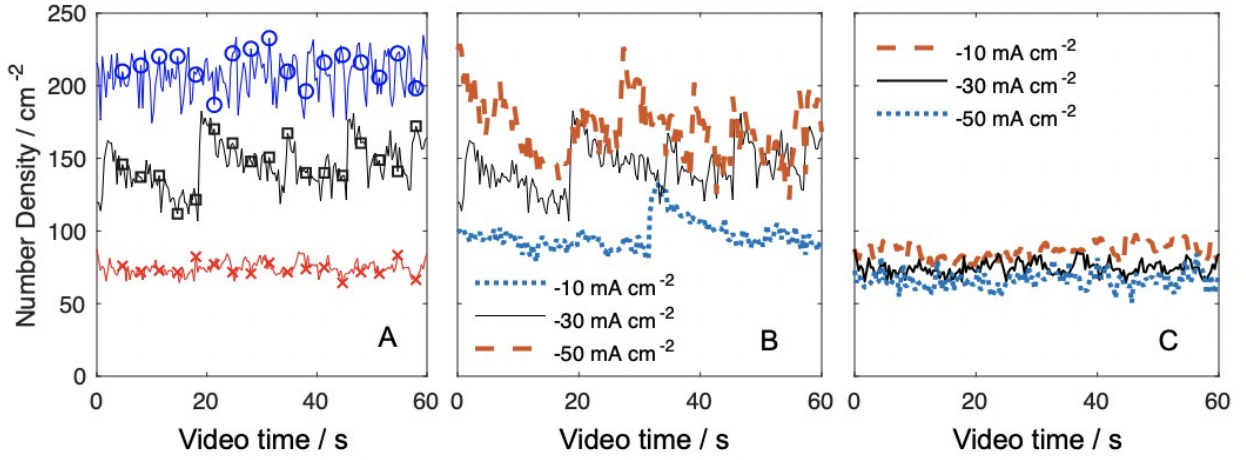

Figure S9: (A) Number density, *N*, of bubbles on the electrode surface as a function of time for planar, μW 6|14, and μW 3|11 n$^+$-Si/Ti/Pt electrodes passing -30 mA cm^{-2} in 0.50 M H_2SO_4(aq) at α = 15° represented by black squares, red x's and blue circles respectively. Number density of bubbles on a (B) planar and (C) μW 6|14 n$^+$-Si/Ti/Pt electrode as a function of time and absolute current density towards H_2.

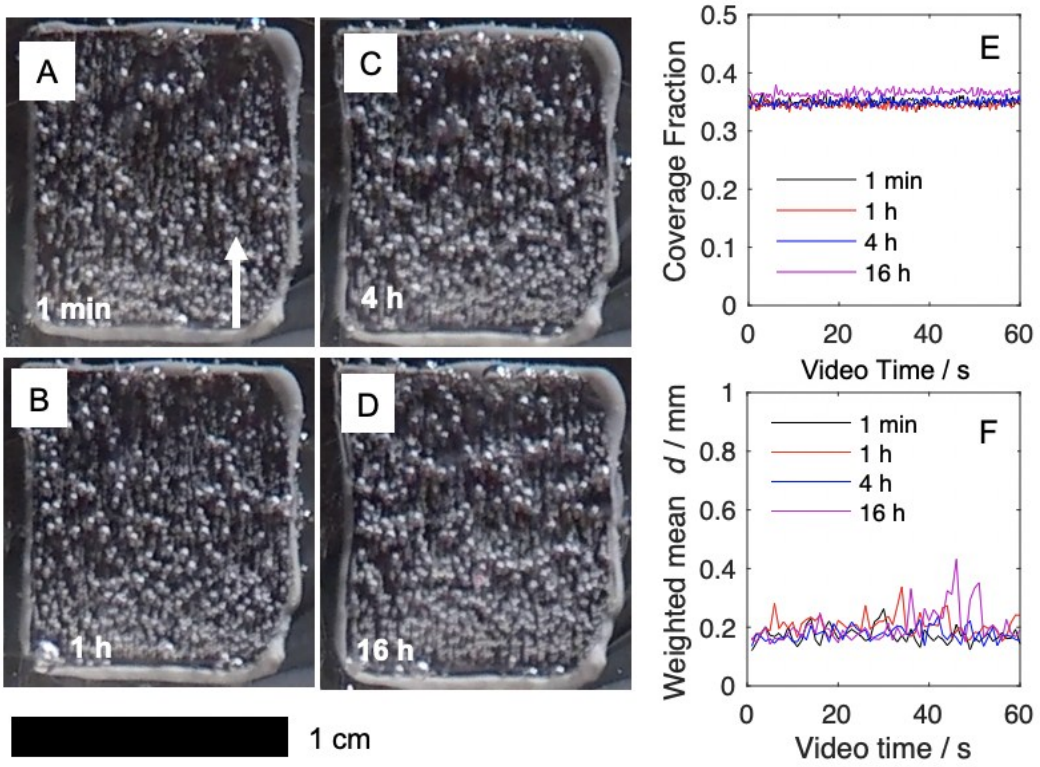

Figure S10: Stability of bubbling behavior for a µW 3|11 electrode in 0.50 M H_2SO_4(aq) at $|^{J_{H_2}}|$ = 30 mA cm^{-2} and α = 15°. Coverage and weighted mean *d* were calculated from videos recorded in 1 min intervals after (A) 1 min, (B) 1 h, (C) 4 h, and (D) 16 hours of electrolysis. (E) Bubble coverage fraction and (F) mean weighted diameter versus time as a function of video start time showed that the behavior of the bubbles was stable during the electrolysis.

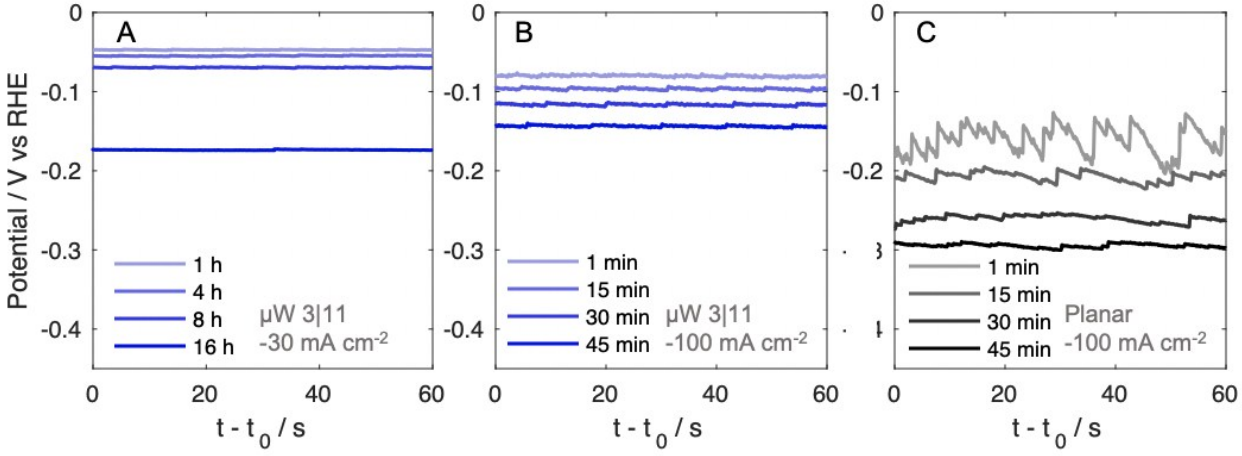

Figure S11: IR-corrected chronopotentiometry data for n^+-Si/Ti/Pt cathodes at α = 15° in 0.50 M H_2SO_4(aq). Traces are sampled for 60 second windows during a constant current experiment for

an extended period of time. (A) µW 3|11 electrode at -30 mA cm^{-2}. (B) µW 3|11 electrode at -100 mA cm^{-2}. (C) Planar electrode at -100 mA cm^{-2}.

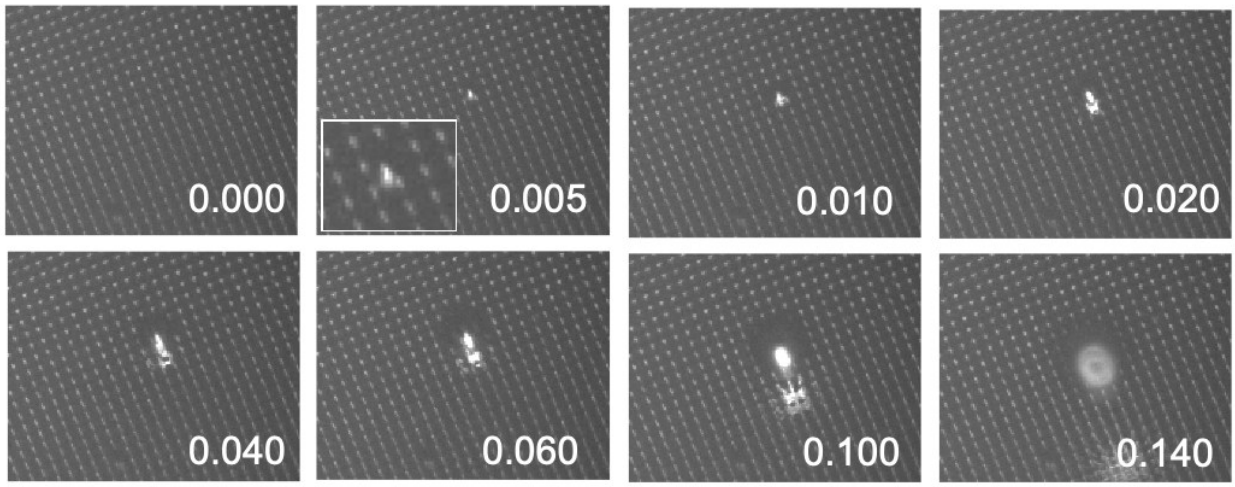

Figure S12: Image sequence at 200 frames s^{-1} and 5-times magnification of an upward-facing µW 6|28 electrode passing 25 mA cm^{-2} of current density for hydrogen evolution. Time stamps are referenced to the first frame and are in seconds. Inset image shows a ~30 µm bubble nucleus forming between microwires. Loss of focus at the bubble surface occurred due to the release from the electrode.

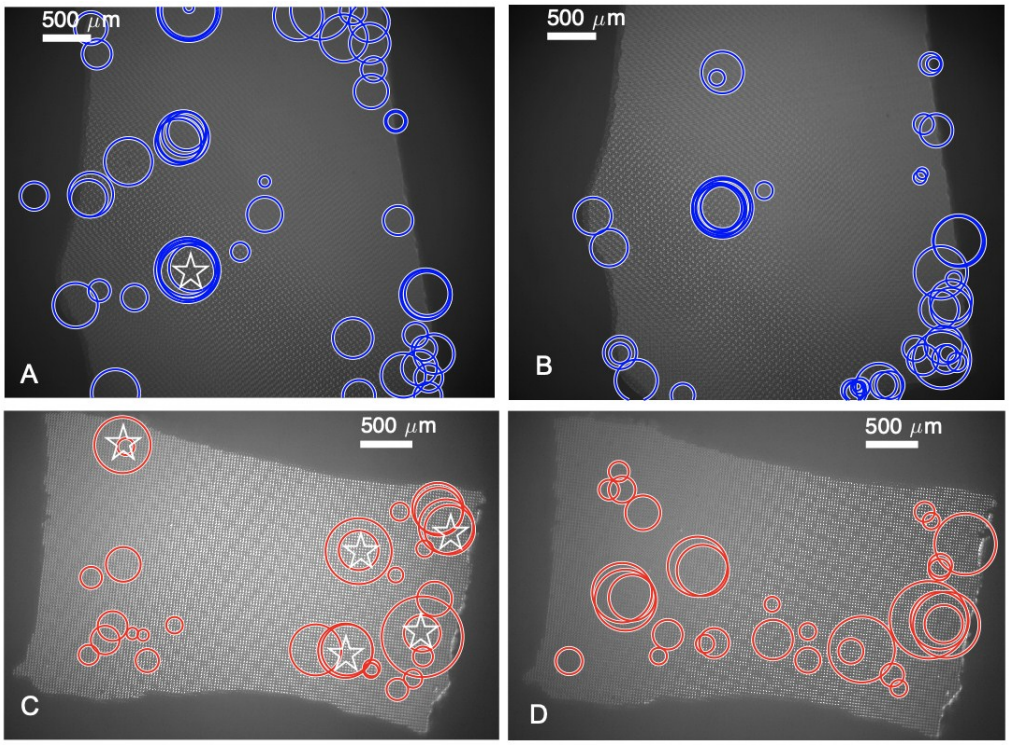

Figure S13: Map of departure diameters measured at µW 6|14 electrode (A,B) and a µW 6|28 electrode (C,D) in an upward-facing configuration passing a constant current density of 50 mA

cm^{-2} towards the HER in 0.50 M H_2SO_4(aq) in two separate experiments. Circles represent individual departure diameters centered on the site of nucleation.

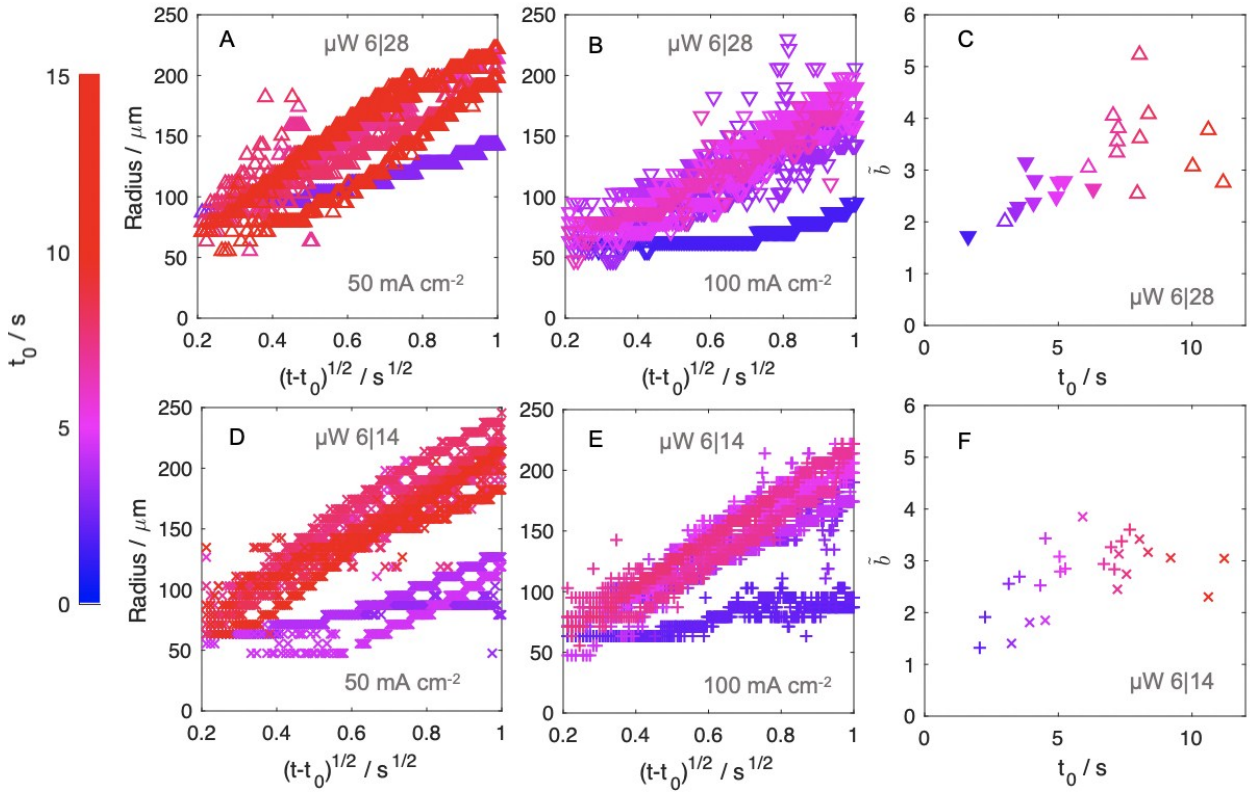

Figure S14: Comparisons of radius versus square root of time traces, where t_0 is the time at nucleation, as measured via image processing software for individual bubbles at an upward-facing μW 6|28 (A,D) and μW 6|14 electrode (D,E). (C,F) Calculated $\tilde{b}$ for data presented in Figure S14A-B and S14D-E, respectively. Growth coefficients asymptotically approached steady state behavior within seconds.

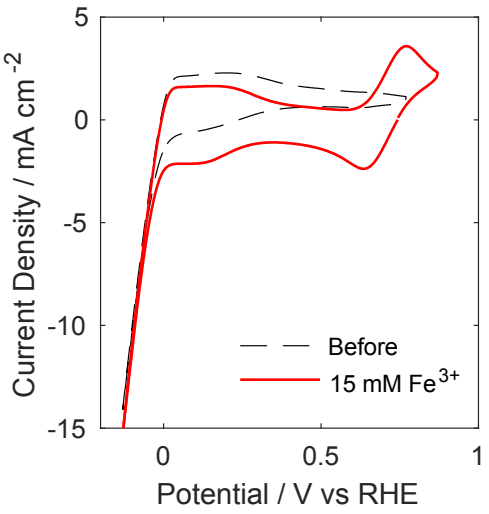

Figure S15: Cyclic voltammograms recorded with a Pt wire in 0.50 M H_2SO_4 (aq) at 500 mV s^{-1} before and after the addition of 15 mM ferric sulfate, shown as black dashed and solid red lines, respectively. The $Fe^{3+/2+}$ redox wave is clearly separated from the potential region for hydrogen evolution and the addition of ferric ions did not influence the onset of hydrogen evolution. The electrochemistry of the one-electron reduction of Fe^{3+} was therefore used as a non-invasive probe of the mass transport characteristics of the electrode in the presence or absence of bubbles due to H_2 evolution.

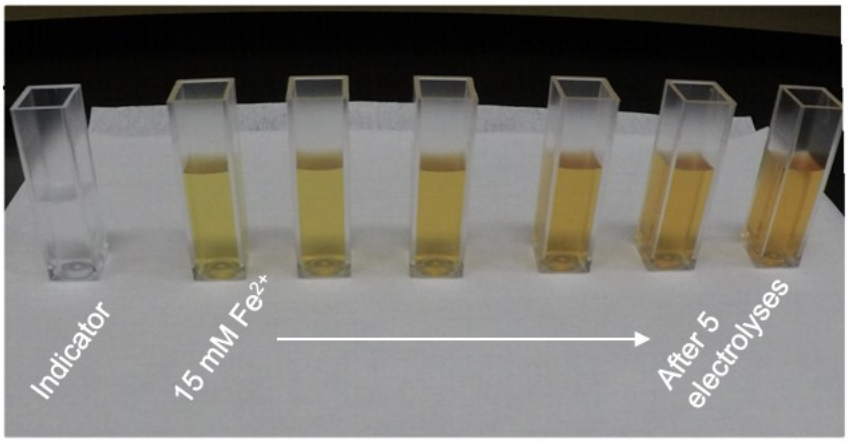

Figure S16: Digital photograph of the effect of increasing Fe^{2+} concentration on the absorbance of a 2.70 mL indicator solution spiked with 0.100 mL of electrolyte (initially, 15 mM Fe^{3+}(aq) in 0.50 M H_2SO_4(aq)).

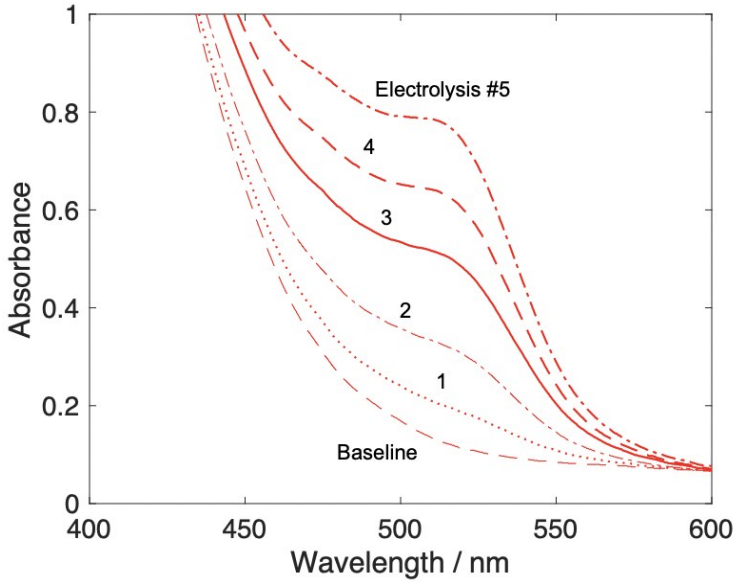

Figure S17: Representative UV-Vis spectra for individual 100 µL samples of $Fe^{3+/2+}$(aq) withdrawn from the electrochemical testing cell, buffered with 0.20 M sodium acetate, and complexed with 1,10-phenanthroline following 5 sequential electrolyses. A baseline spectrum was recorded at 0 C passed.

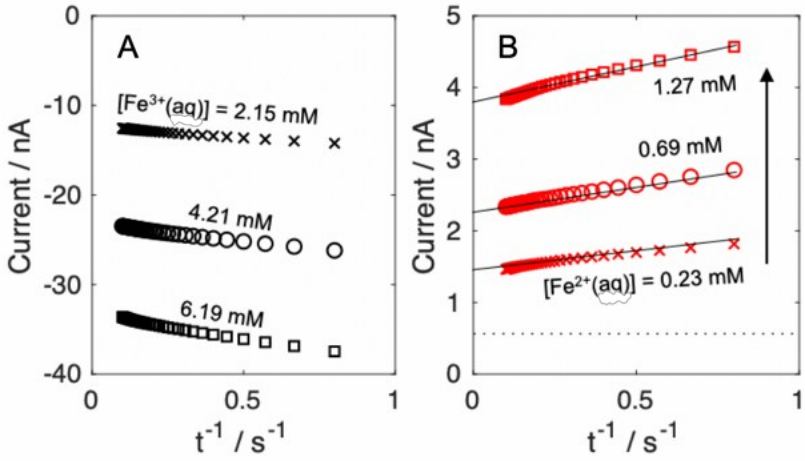

Figure S18: Representative current versus t^{-1} plots at a Au microelectrode in 0.50 M H_2SO_4(aq) with varying concentrations of Fe^{2+}(aq) and Fe^{3+}(aq). (a) Representative cathodic current plots measured at -0.20 V versus the saturated calomel electrode (SCE) after spiking the cell with 1.1 mL aliquots of 100 mM Fe^{3+}(aq) in 0.50 M H_2SO_4(aq). (b) Representative anodic traces measured at 1.00 V vs SCE after sequential electrolyses. Reported concentrations are from spectroscopic measurements after complexation with 1,10-phenanthroline.

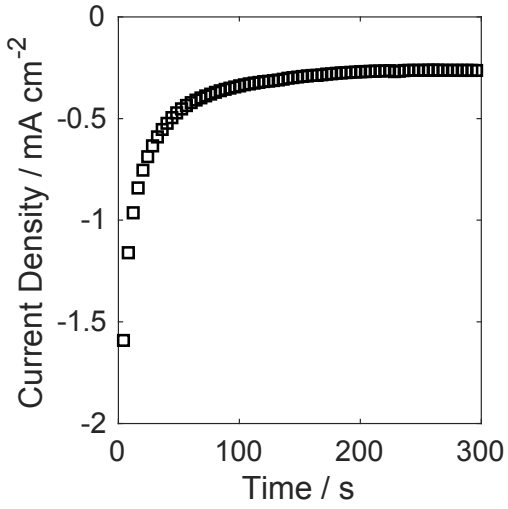

Figure S19: Representative *J* versus t plot for a μW 6|14 electrode held at -0.20 V versus SCE in 0.50 M H_2SO_4(aq) in the presence of 15.0 mM Fe^{3+}(aq) with no external convection and no generation of gas bubbles. The cathodic current density due to diffusion and thermal convection in the cell was < 0.5 mA cm^{-2} after 45 s.

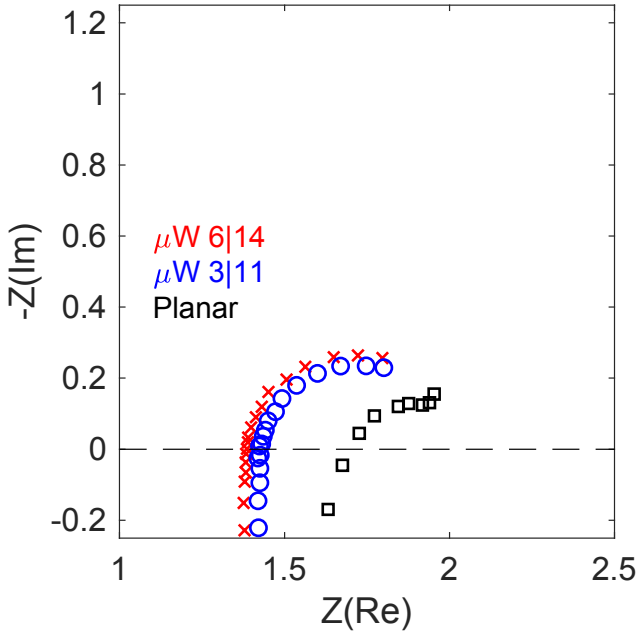

Figure S20: Plot of the imaginary component of the impedance, Z(Im) versus the real component of the impedance, Z(Re) at 0 V versus RHE for frequencies of 100 kHz to 100 Hz at a sampling rate of 6 points dec^{-1}. Z(Re) was not sensitive to frequency from 100 to 50 kHz, where Z(Im) was minimized such that the intercept with the x-axis could be assigned to the ohmic resistance of the cell.

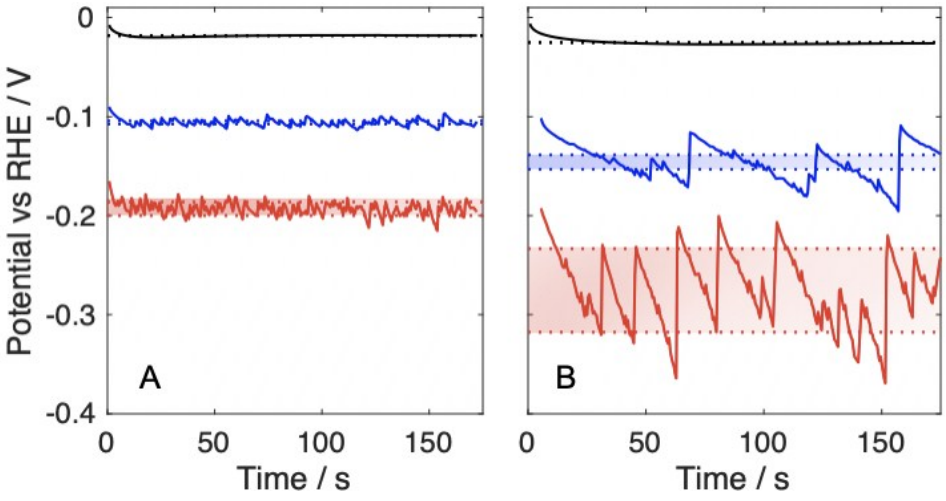

Figure S21: Potential versus time data for a planar Pt electrode at (A) 90° orientation and (B) 15° orientation at 10, 30, and 70 mA cm^{-2}, black, blue, and red lines, respectively. Shaded regions represent the average potential ± one standard deviation in the potential, corrected for ohmic drop, measured via galvanostatic impedance.

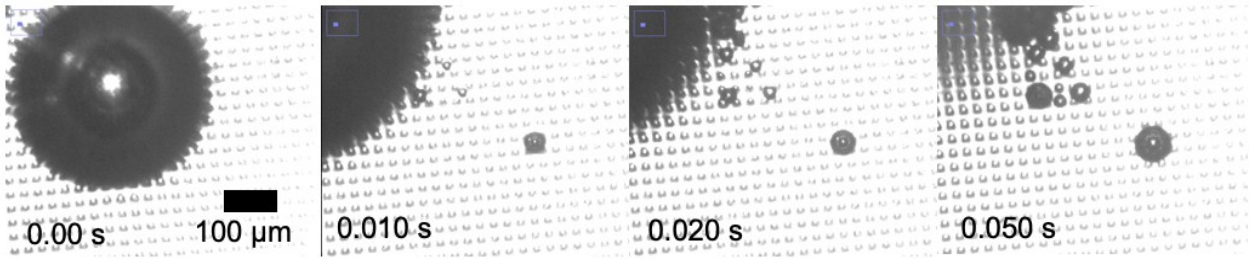

Figure S22: High speed microscope images recorded at an upward-facing µW 6|28 electrode evolving H_2 in 0.50 M H_2SO_4(aq). The departing gas bubble at 0.010 s left multiple nucleation sites within the microwire array.

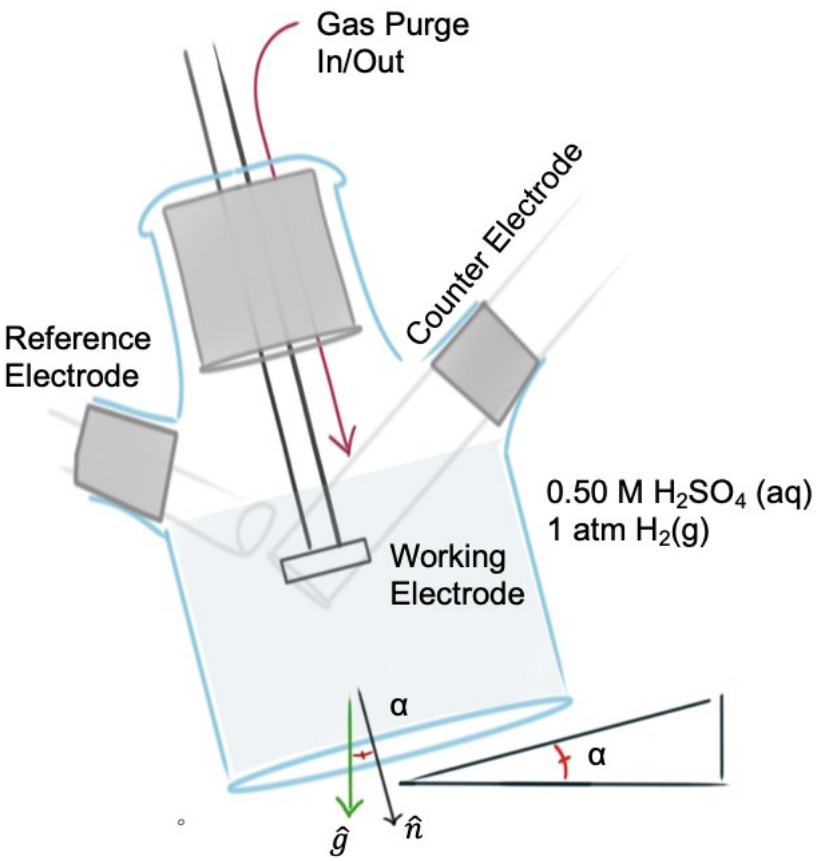

Figure S23: Cell diagram for hydrogen evolution testing.

References

1. W. Fortune and M. Mellon, *Industrial & Engineering Chemistry Analytical Edition,* 1938, **10**, 60-64.

2. A. Harvey Jr, J. Smart, and E. Amis, *Analytical Chemistry,* 1955, **27**, 26-29.

3. X. Wu, E. Yang, and H. Evans, *Journal of Applied Physics,* 1990**, 68**, 2845-2848.

4. P. S. Epstein and M. S. Plesset, M. S., *The Journal of Chemical Physics,* 1950, **18**, 1505-1509.

5. P. van der Linde, A. Moreno Soto, P. Peñas-López, J. Rodríguez-Rodríguez, D. Lohse, H. Gardeniers, D. Van Der Meer, and D. Fernández Rivas, *Langmuir,* 2017**, 33**, 12873-12886.